Superficial severe plastic deformation of 316 LVM stainless steel through grit blasting: Effects on its microstructure and subsurface mechanical properties

M. Multigner [a,b](*), S. Ferreira [a], E. Frutos [b,a], M. Jaafar [c], J. Ibáñez [a], P. Marín [d], T. Pérez-Prado [e], G. González-Doncel [a], A. Asenjo [f], J.L. González-Carrasco [a,b]

[a] *Centro Nacional de Investigaciones Metalúrgicas, CENIM-CSIC, Avda. Gregorio del Amo 8, 28040 Madrid, Spain*
[b] *Centro de Bioingeniería, Biomateriales y Nanomedicina, CIBER-BBN, Instituto de Salud Carlos III, Spain*
[c] *Dpt. Física de la Materia Condensada, Fac. Ciencias, UAM, 28040 - Madrid, Spain*
[d] *Instituto de Magnetismo Aplicado (RENFE-UCM-CSIC), P.O. Box 155, 28230 Las Rozas, Madrid, Spain*
[e] *Madrid Institute for Advanced Studies of Materials (IMDEA-Materials) c/ Profesor Aranguren s/n, 28040 - Madrid, Spain*
[f] *Instituto de Ciencia de Materiales de Madrid, CSIC, 28040 - Madrid, Spain*

ABSTRACT

The microstructure and mechanical properties of austenitic stainless steel 316 LVM (Low Vacuum Melting) blasted with either small and rounded ZrO_2 particles or larger and angular shaped Al_2O_3 particles is analysed through Magnetic Force Microscopy, Synchrotron Radiation Diffraction and Ultramicroindentation techniques. It is shown that blasting causes a severe plastic deformation that roughens the surface and produces a significant sub-surface grain refinement and work hardening. The gradient in the plastic deformation and the volume increase associated with the deformation induced α´-martensite accounts for the development of compressive residual stresses with a maximum value close to the surface. All these features yield a gradient in hardness with a maximum value beneath the surface. Compared with the Al_2O_3 particles, the ZrO_2 particles cause a higher value of compressive residual stress and a lower increase in hardness. Also, the Al_2O_3 particles lead to more α´-martensite formation at deeper regions from the surface than the ZrO_2 particles. The different results are related with the specific morphology of the particles and their specific role in the blasting process.

(*)Present address: Instituto de Magnetismo Aplicado (UCM-ADIF-CSIC), P.O. Box 155, 28230 Las Rozas (Madrid) Spain.

1. Introduction

In many applications, material surface preparation for optimal performance is required. Examples of these uses include: surface cleaning from grease or paint, surface roughness generation (for anchoring thermally sprayed coating [1], improving the mechanical stability of implants [2]), generation of superficial (compressive) residual-stress to improve fatigue behavior [3], etc. Different processes are presently available to achieve the above objectives, and the appropriated procedure should be employed depending on the specific use. The common basic feature of all of them is the bombardment of energetic particles (projectiles) onto the material to modify its surface. The main difference among them resides in the type (nature) of particles employed. These are various, and can be, for example: angular shaped metallic or ceramic particles (grit blasting), rounded shape metal or ceramic particles (shot peening), or ceramic particles, regardless of their shape (sandblasting). In particular, blasting with ceramic particles has proved to be very useful to confer roughness on the surface of materials. For this reason, it is commonly applied to biomaterials for orthopaedic applications, since rough surfaces present better bone fixation than polished ones [2].

As mentioned above, the consequences of a given surface treatment are defined mainly by the particle´s nature (*e.g.*, angular shaped particles lead to more material removal than rounded ones [4]). However, the target and the parameters used in the process also determine the changes experienced by the material's surface. For example, the incident angle influences noticeably the depth of the compressive residual stress generated [5]. It is also worth mentioning that the surface modification pursued by a given process is always accompanied, to a greater or less degree, by the other effects of particle bombardment. For instance, sandblasting confers surface roughness and also sub-surfaces features influencing their microstructure and residual stress state. The

overall picture of the consequences resulting from blasting with ceramic particles should, therefore, be evaluated for materials use and in particular in biomedical applications. However, such studies have rarely been done.

Research into the effect of blasting for bio-medical applications has been mainly focused on Ti and Ti-base alloys [6,7,8] . Studies on austenitic steels are, however, scarce [9]. Austenitic stainless steel 316 LVM is being used as a biomaterial, since it combines good mechanical properties with reasonable biocompatibility. Its low cost and easy machining has also permitted its development as a biomaterial, leading at present, to the manufacture of a great variety of components for implants. In particular, the fabrication of screws from stainless steels is, now, possibly the most common use of this alloy in orthopaedic surgeries.

The present study covers, hence, an overall picture of the sub-superficial microstructural and mechanical properties of the austenitic stainless steel 316 LVM as a consequence of blasting with two different types of particles, namely, micro-spheres of ZrO_2 (125-250 μm in size) and angular Al_2O_3 particles (~750 μm size). Such research is of great significance due to the present interest in this alloy for bio-medical uses. Furthermore, it will be shown that conventional blasting with ceramic particles may lead to microstructures and mechanical properties which are close to those achieved by more sophisticated versions of this process, such as Surface Severe Plastic Deformation (S^2PD) processes [10 and references therein,11,12].

2. Experimental Details

For this research we have used specimens removed from a 316 LVM austenitic stainless steel bar, whose chemical composition (wt%) is Cr 17.48, Ni 14.13, Mo 2.87, Mn 1.62, Si 0.53, C 0.024, Cu 0.067, N 0.061, S 0.001, and Fe in balance. Disks of 20

mm in diameter and 2 mm thick were blasted by the implant manufacturer (Surgival SL, Valencia, Spain).

Blasting was performed with two different types of particles under a pressure of 350 KPa for 2 minutes and the distance between the nozzle and the target surface was 20 cm. A first set of samples, hereinafter BL_ZrO, has been blasted using ZrO_2 embedded in silica vitreous phase microspheres sized between 125 μm and 250 μm. The second set of samples, hereinafter BL_AlO, has been blasted with alumina angular particles (white corundum) of around 750 μm size. Table 1 shows properties of the blasting particles and the nomenclature used.

In order to preserve the original blasted surface during sectioning and to avoid artefacts during the measurements performed beneath the surface, selected specimens were electrolytically coated with a fine layer of Cu.

Roughness of the as-processed specimens was determined with a profilometer Mitutoyo Surftest 401 averaging 3 measurements of 4 cm in length. For comparative purposes, unblasted specimens were ground with consecutively finer SiC papers, and finely polished with diamond paste and colloidal silica (0,5 μm) to remove all disturbed metal. The steel's microstructure was characterized using both X-ray diffraction and scanning electron microscopy (SEM). Microstructural characterization of the surface morphology and cross sections of the specimens was carried out by using a scanning electron microscope (JEOL-6500F) equipped with a field emission gun and coupled with an energy dispersive X-ray (EDX) system for chemical analysis. The grain structure was revealed by Backscattered Electron Images obtained on fresh grinding and polished surfaces as previously described.

The contrast of the image is associated with the different crystallographic orientation of the grains, since in this case, heterogeneities in composition are not

expected. Electron backscattered diffraction (EBSD) using the HKL Channel 5 software made it possible in addition to detect elastic lattice distortions. The acceleration voltage was 20 KeV. Sample preparation for EBSD examination consisted of grinding and polishing as previously described.

To evaluate the formation of strain induced α´-martensite, X-ray diffraction (XRD) measurements were carried out with Co K_α radiation in a Bruker AXS D8 diffractometer in grazing incidence condition, with a beam incidence angle of 1º and 2θ scan between 35 and 115º with a step size of 0.03º over the blasted surface. The Rietveld method is a powerful tool for the calculation of structural parameters from diffraction patterns. For the application of the Rietveld method to grazing incidence X-ray diffraction (GIXRD) instrument functions were empirically parameterised from the profile shape analysis of a corundum sample. This was measured under grazing incidence with the same conditions. In this study, we have used the version 4.0 of Rietveld analysis program TOPAS (Bruker AXS) for the XRD data refinement.

Residual stress depth profiles have been measured by energy dispersive diffraction using synchrotron X-Ray radiation on EDDI beam line at BESSY, Berlin, Germany, which operates in the range 10-150 KeV. The use of energy dispersion makes it possible to detect many diffraction peaks. Measurements were carried out in reflection mode using an angle 2θ = 9º. The incoming beam was defined by slits of 1mm height and 1mm width, while the diffracted beam size was adjusted by slit of 30 μm (gauge volume: 1mm × 1 mm × 0.03 mm). The so-called *sin2ψ* method [13] has been used. A Biaxial RS state approach is assumed, i.e.: $\sigma_{i3}(z = 0) = 0 \ (i = 1, 2, 3)$. The local (total) stress changes with the depth on the surfaces, and then the residual stress condition (in-plane stresses) obeys a biaxial state [14].

The mechanical properties were evaluated through ultra-microindentation experiments performed with a Nanotest-MicroMaterials equipment (Nanotest-600) using a Berkovich three-sided pyramidal indenter. The measured depth was adjusted taking into consideration the effect of the instrument compliance (0.52973 nm/mN). After calibration, the instrument was set up for fifteen series of indentations on the cross sections, along directions parallel to the sand blasted surface. Indentations were measured through the control depth, to a depth fixed at 490 nm. The loading and unloading speed was 0.75 $nm.s^{-1}$. The dwell periods at the maximum load and for the drift correction were 5 and 30 seconds, respectively. All experiments were performed at 23ºC. Calculation of the hardness and the Young's modulus was made by the model proposed by Oliver & Pharr [15].

Hysteresis loops have been obtained to compare the amount of strain induced α´-martensite (magnetic) phase resulting after blasting with different blasting particles. For these measurements, a vibrating sample magnetometer PPMS-VSM Quantum Design working at 300 K and with a maximum magnetic field of 2T, was employed. Samples consisted of small pieces of approximately 4x2x2 mm, which were mechanically removed from the disks, leading to a sample with three blasted surfaces.

The distribution of this phase in the subsurface has been studied by magnetic force microscopy (MFM) in cross-section of samples. Combined atomic force microscope (AFM) and magnetic force microscope imaging have been performed using a microscope from Nanotec Electrónica S.L. The topography of the surface (AFM) and the magnetic image are acquired simultaneously in dynamic mode [16]. Nanosensors Standard and Low Moment MFM probes with a force constant of 3 N/m and a resonance frequency of 75 KHz have been used in these experiments [17]. This technique, unlike the transmission electron microscopy, makes it possible to detect the

α´-martensite phase even in nanocrystalline size without the need for any special preparation.

3. Results

3.1 Microstructure

3.1.1 SEM

SEM examination reveals that blasting causes the plastic deformation of the alloy surface, resulting in an irregular morphology with an average roughness, Ra, of 0,9 μm and 6,7 μm for BL_ZrO and BL_AlO samples, respectively. A close examination reveals the presence of bright zones containing large particles of heterogeneous size, (Fig. 1), that EDX analysis detects as remnants of the blasting particles. On one hand blasted Al_2O_3 particles present polygonal edges and are often broken, forming agglomerates of fine particles (Fig 1B). On the other hand, ZrO_2 particles on BL_ZrO specimens present soft edges and seem to be plastically deformed (Fig 1A).

The microstructure of the subsurface is also modified by the process (Figs. 2 A and B) showing a grain size gradient that achieves sizes in the sub-micrometric range in the near surface (Figs. 2 C and D). Heterogeneities in the grain size distribution can be detected inside the sub-micrometric area, with areas in which the grain size is about 500 nm (labelled as "1" in Figs. C and D) and other areas with grains under 100 nm (labelled as "2").

Three zones can be distinguished in both samples although the limits are not well defined and the depths of each vary from one to another (Figs. 2A and B). The zone just beneath the surface (10-15 μm) is characterized by an ultrafine microstructure (Figs. 2 C and D). The next zone (about 50 μm depth) presents highly deformed grains,

as well as twins and martensite needles without well defined grain frontiers (Figs. 2 E and F). The third and deepest zone shows a progressive change in the backscattered signal, which shows a slight change in the crystallographic orientation. The grains are not altered for depth more than 100 μm and 200 μm for BL_ZrO and BL_AlO, respectively.

3.1.2. XRD

GIXRD patterns of the blasted samples, Fig. 3, show the existence of low intensity reflections of α'- martensite phase, in addition to the dominant austenite peaks. It can also be observed that the relative diffracted intensity ratio of α'-martensite phase to austenite phase is slightly lower in the BL_AlO specimens than in the BL_ZrO ones. In the GIXRD patterns of Fig. 3 the broadening of the diffraction Bragg peaks in the blasted samples with respect the polished sample can also be clearly observed. This suggests a progressive decrease of the grain size and/or increase in lattice strain. However, due to the through-the- thickness microstructure variation of the (Fig. 2), it was not possible to calculate a mean crystallize size and strain value. It has been estimated that 70 % of the Cu Kα radiation signal for 1º of incidence angle into 316 LVM stainless steel comes from a layer of about 100 nm [18]. In this case, however, less energetic Co radiation has been used, suggesting that the diffracted signal is associated with a thinner superficial layer. The lattice parameter obtained from the Rietveld analysis is a_γ =3.599 Å for austenite phase (fcc) and a_α= 2.878 Å for α´-martensite (bcc) [19]. In the case of the austenite, the (111), (200), (220) and (311) reflections were used for this calculation. As shown in Fig.3, for the blasted samples the X-ray diffraction peak of γ-Fe at about 59° (200) is observed at lower angles than for the polished one, being the effect not visible in the ~ 52° peak. This

effect has been associated to the presence of planar defects and in the present case they might be stacking faults since deformation induced martensite is formed by blasting [20, 21].

3.2 Residual Stress

3.2.1 Synchrotron radiation diffraction

Depth profiles of the in-plane residual stresses evaluated from the $sin^2\psi$ data obtained by energy dispersive diffraction are shown in Fig. 4. The graph shows, first, that residual stresses are clearly present in the samples processed using both alumina and zirconia particles. For the reference sample, polished condition, small uniform compressive stresses of about - 100 MPa (average value) were detected. In the case of BL_ZrO, the magnitude of the maximum compressive residual stress (-670 MPa) is higher than the sample blasted with alumina BL_AlO (- 470 MPa). The shape of the residual stress profile of the sample blasted with ZrO_2 particles is similar to that obtained by shot peening with metallic shot [22], although the depth reached is much smaller for the ceramic balls, as was expected. The profile of the BL_AlO is more flattened and is characterized by lower residual stresses as obtained in low carbon steel surfaces with this kind of blasting particles [1].

3.2.2 EBSD

The presence of residual stresses was also demonstrated by EBSD in both BL_AlO and BL_ZrO samples. As an example, Fig. 5 illustrates the band contrast map corresponding to the area of interest of BL_AlO sample. Gray tones in band contrast maps such as those of Fig. 5 represent the quality of the corresponding Kikuchi patterns, which can be related to the presence of elastic strains. Darker tones correspond to lower

quality patterns, i.e., to higher strains. A highly non homogeneous distribution of elastic stresses can be noticed. Some areas (such as number 1 in the figure) do not seem to have significant residual stresses, while others (numbers 2 and 3) clearly show the presence of elastic stress gradients.

Black areas are associated with either grain boundaries or to regions with a large density of dislocations. It can be seen that these areas are located close to the surface.

3.3 Microhardness

In the absence of any surface treatment and any change in the crystalline structure that could introduce hardening effects, the hardness and reduced modulus of stainless steel 316 LVM, assuming a Poisson's ratio of 0.3, to a maximum indentation depth of 490 nm has been measured to be 6.1 ± 0.2 and 220 ± 0.2 GPa, respectively. However, as can be observed in Fig. 6, blasting produced a hardening near the surface that extends to about 150 μm and 100 μm into the bulk, depending on whether the blasting was performed with particles of Al_2O_3 or ZrO_2, respectively. The maximum hardness value measured in both cases is about 9.8 GPa, that means a hardness increase of about 60 % with respect to the bulk value. Such increase is significant if it is compared with those obtained with sophisticated techniques such as surface mechanical attrition treatment (SMAT) [23]. It can also be observed that for the same depth, hardness is higher for the BL_AlO sample, except in the very near surface region where the tendency changes. These results indicate that the larger angular particles (BL_AlO) should not only introduce a more extensive subsurface modification, but also a greater hardening [24].

3.4 Magnetic properties

As α´-martensite is a ferromagnetic phase and austenite not, the presence of the former should be easily detected by a hysteresis loop. Fig. 7 shows that both blasted samples have a similar ferromagnetic signal (the paramagnetic signal of the austenite phase has been subtracted). Since the blasted samples have a quite similar volume and surface affected zone and they have almost the same saturation magnetization, it can be concluded that both samples have approximately the same quantity of α´-martensite phase.

Coercive field of the BL_ZrO sample is higher, 120 Oe, than that for the BL_AlO one, 65 Oe. SEM images (Fig. 2) have shown that martensite needles have lengths of tens of microns. Considering that magnetic materials of this morphology are multidomains, it can be assumed that grain size of α´-martensite developed in the BL_ZrO samples should be smaller [25].

3.5 MFM

MFM studies of these samples extends the information about α'-martensite distribution in the near surface region, i.e. it allows us to understand the relationship between the mechanic and magnetic properties in both blasted samples. In the MFM images, dark and bright contrasts appear in certain regions of the samples. Dark contrast corresponds to attractive tip-sample interactions, while bright contrast can be associated with the regions where there is a repulsive tip-sample interaction. No correlation between topography and magnetic signal has been found, i.e. we can assume that the polishing process is not responsible for the magnetic behaviour.

The blasted surfaces have been systematically studied by this technique. Figs. 8A and 8B show, respectively, the topography (AFM) and the magnetic (MFM) images of the subsurface of BL_ZrO. It can be seen that in the first microns, submicrometric (as

shown in Fig. 2) α´-martensite (black and white contrast) coexist with submicrometric austenite characterized by the absence of magnetic signal.

Fig. 9 shows images, with different magnifications, of an area placed at about 10 μm from the surface of a BL-ZrO sample. It can be seen that α´-martensite is heterogeneously distributed along parallel and perpendicular directions to the surface. Along the perpendicular direction, and beyond 25 μm from the surface, martensite is not detected. However, as we get closer to the surface, higher density of the magnetic phase is observed. Along the parallel direction, areas of high density of magnetic phase intercalate with areas of a lower density.

In the transition area from the ultrafine to the non-affected microstructure typical α´-martensite needles can be found. Such lines present bright and dark contrast that corresponds to multidomain regions. The parallels lines appear in different directions as is also observed in the SEM micrographs (Fig 2). In addition, dark spots that correspond to single domain crystals can also be found. Some "magnetic zones" present single domain configuration with low coercive fields i.e. the magnetization in these regions will be always oriented parallel to the tip stray field, presenting homogeneous dark contrast. In Fig. 10 an MFM image has been superposed on the SEM image and it can be checked that the magnetic domains organised in lines match reasonably well with the metallographic α´-martensite needles [11].

In the BL_AlO sample the magnetic contrast appears in deeper regions (Fig 11), even at 40 μm from the surfaceThe MFM images also reveal the existence of multi domains and single domain regions (Fig. 11C and D) but there are more of the latter ones than in the BL_ZrO samples. Another difference with the BL_ZrO samples is that there are less areas showing magnetic contrast close to the surface, which means that

there are less α´-martensite phase just under the surface in the case of the BL_AlO sample.

4. Discussion

It has been shown that blasting of 316 LVM with either of the two types of particles used in this research can produce a very small grain size, ranging between 50 and 500 nm just underneath the surface, in a layer of about 10-15 μm. Furthermore, some mechanical properties, such as microhardness and compressive residual stress of 316 LVM stainless steel, are enhanced with blasting treatment. The grain size achieved in some regions as well as the mechanical properties is comparable to those obtained with S^2PD techniques [11,12,21]. For example, about a 60 % increase in microhardness is achieved, which is of the same order of magnitude as those obtained by SMAT in 316 L stainless steel (figure 6 of reference [23]). It is also remarkable that about 670 MPa of compressive residual stresses is achieved with blasting, which is similar to the value of 550 MPa for the shot-peened AISI 304 [26] or to the residual stress values calculated for different S^2PD processes that range between 60 and 650 MPa [27]. It is worth noticing that the main contribution to hardening is attributed to residual stresses introduced by blasting with ceramic particles [28].

Despite the fact that both types of particle lead qualitatively to similar surface effects on the blasted 316 LVM stainless steel, the overall picture of the results obtained is, however, quite different depending on the particles used. These differences should be understood within the framework of the specific features that distinguish the ZrO_2 and Al_2O_3 particles. As mentioned above, the ZrO_2 particles are rounded and of about 250 μm in size, whereas the Al_2O_3 ones are some three times larger and have a rough surface characterized by edge-like facets. Two of the consequences are: a) the ZrO_2

particles produce a more homogeneous deformation than the Al_2O_3 ones and b) the ZrO_2 particles barely lead to grinding down the material, unlike the Al_2O_3 ones.

On the other hand, the largest Al_2O_3 particles are also more energetic and, therefore, lead to more cumulative deformation, which implies more strain hardening and to the formation of α´-martensite at deeper regions from the surface. This is in agreement with the trends shown in Fig. 5 and MFM results. A higher level of in-depth residual stress in the BL_AlO than in the BL_ZrO_ samples would also be expected. Some of these large particles, however, lead to a micro-cutting effect. We assume that in these cases no plastic deformation on the surface occurs, since virtually all impacting energy is devoted to tearing off material. Hence, some of the α´-martensite accumulated from previous impacts (which do not erode material) is also eliminated from the surface. This erosion effect, besides some α´-martensite removal, also results in some residual stress relaxation, in the same way as a macroscopic residual stress of a given sample relaxes when it is sectioned into several pieces. As a consequence, the maximum absolute residual stress value (obtained at ~10 -20 μm) is lower in the BL_AlO sample than in the BL_ZrO one due to stress relaxation. At lower regions, however, the residual stresses are higher. In addition, this also explains the more heterogeneous distribution of the α´-martensite on the surface of the BL_AlO samples.

It is worth noting that the cumulative impact effect is necessary to produce α´-martensite formation, since a given threshold strain level is needed for the transformation. Obviously, this increasing transformation process is retarded when local material removal by the large and edge-like Al_2O_3 particles occurs.

The local temperature increase, due to particle impact, can also be invoked as a possible source of residual stress relaxation and to the reversion of the α´-martensite into austenite. A minimum of about 510ºC is required for such a reversion [29].

Similarly to that observed during shot-peening of the Ti6Al4V alloy [30], where the temperature reached up to about 700 ºC, temperature at the blasted surfaces is expected to increase. In our case, however, the temperature reached during blasting has not been monitored. Therefore, we cannot make any conclusions about this possibility.

A final consideration concerns the effect blasting on relevant surface related properties, such as fatigue and corrosion resistance, which are beyond of the aims of this work. The ultrafine-grained subsurface microstructure and the compressive residual stress induced by the severe surface plastic deformation would be beneficial for the fatigue resistance by impeding dislocation movement and delaying crack initiation [31]. The outer fine-grained layer would yield good corrosion resistance because the high amounts of grains boundaries would enable fast diffusion of Cr to the surface [32]. Besides, it is known that the corrosion behaviour of stainless steels can deteriorate substantially when the volume fraction of the strain-induced martensite increases, because the structural inhomogeneities would increase the density of the localized states [33]. Therefore, the effect that the submicrometric α´-martensite could produce on the corrosion response should be also studied to deepen the biological response of this biomaterial after this surface treatment.

5. Conclusions

- Blasting of austenitic stainless steel with either alumina or zirconia particles produces a severe surface plastic deformation that roughs the surface and produces a grain size refinement, ranging between 50 and 500 nm in a layer of about 10 -15 μm beneath the blasted surface, and ~ 45 μm for the bulk.

- Following the ultrafine-grained zone, highly deformed grains containing twins and strain induced α´-martensite needles are found.

- Compressive residual stresses with maximum absolute values close to the blasted surfaces are found. Depth profiles obtained by synchrotron diffraction show that values for the specimens blasted with zirconia particles (~ 670 MPa) are higher than those for specimens blasted with alumina (~ 470 MPa).

- Subsurface hardening, with a maximum hardness value beneath the blasted surface, extends to about 150 and 100 μm into the bulk for the alumina and zirconia blasted specimens, respectively. Overall, hardening is higher when blasting with the alumina particles, probably due to their greater hardness and larger size. The net effect is a more effective subsurface work hardening and formation at deeper regions from the surface of strain induced α´-martensite.

- The angular shape of the alumina particles causes severe erosion that grinds down the material, leaving the surface with a higher roughness. This erosion effect, besides some α'-martensite removal, results in some residual stress relaxation. Thus values are lower than those determined for the zirconia blasted specimens, for which a more homogeneous deformation was observed.

Acknowledgements

The authors wish to express their thanks for the financial support of the Spanish Projects MAT2006-12948-C04-01, MAT 2009-14695-C04-02-04 and the CIBER-BBN of Bioingeniería, Biomateriales y Nanomedicina, supported by the ISCIII. Dra M.M. thanks grants of "Juan de la Cierva" (MICINN) and JAE-DOC (CSIC). The authors

thank J.A. Jiménez for the X ray measurements help and the ICMM-SPM Service for the AFM/MFM measurements.

References

[1] K. Poorna Chander, M. Vashidta, K. Sabiruddin, S. Paul, PP. Bandyopadhyay, Mater. Des. 30 (2009), p. 2895.

[2] D.A. Puleo and M.V. Thomas Dent Clin North Am 50 (2006), p. 323.

[3] I. Altenberger, B. Scholtes, U. Martin, H. Oettel, Mater. Sci. Eng. A 264 (1999), p. 1.

[4] J.E. Goodwin, W. Sage, G.P. Tilly, Proc. Instn. Mech. Engrs. 184 (1969-70), p. 279.

[5] T. Hong, J.Y.Ooi, B.Shaw, Eng. Fail. Anal. 15 (2008), p. 109.

[6] X.P.Jiang, X.Y.Wang, J.X.Li, D.Y. Li, C.S. Man, M.J.Shepard, T. Zhai, Mater. Sci. Eng. A 429 (2006), p. 30.

[7] C. Leinenbach and D. Eifler, Biomaterials 27 (2006), p. 1200.

[8] M. Multigner, E. Frutos, C.L. Mera, J. Chao, J.L. González-Carrasco, Surf. Coat. Tech. 203 (2009), p. 2036.

[9] M. Multigner, E. Frutos, J.L. González-Carrasco, J.A. Jiménez, P. Marín, J. Ibáñez, Mater. Sci. Eng. C 29 **(**2009), p.1357.

[10] A.L. Ortiz, J.W. Tian, J.C. Villegas, L.L. Shaw, P.K. Liaw, Acta Mater. **56** (2008), p. 413.

[11] H.W. Zhang, Z.K. Hei, G. Liu , J. Lu , K. Lu, Acta Mater. **51** (2003), p. 1871.

[12] X.Y. Wang, D.Y. Li, Wear 225 (2003), p. 836.

[13] I.C. Noyan and J.B. Cohen, Residual Stress. Measurements by Diffraction and Interpretation, Springer, New York, (1987).

[14] Ch. Genzel, C. Stock,W. Reimers, Mater. Sci. Eng. A 372 (2004), p. 28.

[15] W.C. Oliver, G. M. Pharr, J. Mater. Res. **7** (1992), p. 1564.

[16] A. Asenjo, J.M. García, D. García, A. Hernando, M. Vázquez, P. Caro, D. Ravelosona, A. Cebollada, F. Briones, J. Magn. Magn. Mater. 196 -197 (1999), p. 23.

[17] M. Jaafar, A. Asenjo and M. Vázquez, IEEE Trans. Nanotechnology **7** (3) (2008), p. 245.

[18] J. Dudognon, M. Vayer, A. Pineau, R. Erre, Surf. Coat. Technol. 200 (2006), p.5058.

[19] R. Reed, Acta Metall. 10 (1962), p. 865.

[20] B.E. Warren, X-Ray Diffraction, Addison-Wesley, Reading, MA,1969, Chapter 13.

[21] P. Sahu, M. De, S. Kajiwara, J. Alloys Compd. 346 (2001) 158.

[22] D.J. Buchanan and R. John, Scripta Mater. 59 (2008), p. 286.

[23] T. Roland, D. Retraint, K. Lu, J. Lu, Mater. Sci. Eng. A 445 (2007), p. 281.

[24] T. Hong, J.Y.Ooi, B. Shaw, Eng. Fail. Anal. 15 (2008), p. 1097.

[25] B.D. Cullity, Introduction to magnetic materials, Addison-Wesley, Reading, MA,1972, Chapter 11. [26] I. Altenberger, B. Scholtes,U. Martin, H. Oettel, Mater. Sci. Eng.A 264 (1999), p. 1.

[27] K. Dai and L. Shaw L, Mater. Sci. Eng. A 463 (2007), p. 46.

[28] E. Frutos, M. Multigner, J.L. González-Carrasco, Acta Mater. 58 (2010) p. 4191.

[29] S.J. Lee, Y.M. Park, Y.K. Lee, Mater. Sci. Eng. A 515 (2009), p. 32.

[30] L. Reissig, R. Völkl, M.J. Mills, U. Glatzel, Scripta Mater. 50 (2004), p. 121.

[31] T. Roland, D. Retraint, K. Lu, J. Lu, Scripta Mater. 54 (2006), p. 1949.

[32] B.N. Mordyuk, G.I. Prokopenko, M.A. Vasylyev, M.O. Lefimov, Mater. Sci. Eng. A 458 (2007), p. 253.

[33] A. Cigada, B. Mazza, P. Pedeferri, G. Salvago, D. Sinigaglia, G. Zanini, Corros. Sci. 22(6) (1982), p. 558.

Figure captions

-Figure 1. Surface micrographs of Bl_ZrO (A), Bl_AlO (B) and polished sample (C). A) At the center of the image a rest of a ZrO_2 blasting particle can be observed. B) Arrows indicate the rests of Al_2O_3 blasting particles.

- Figure 2. Cross section micrographs of Bl_ZrO (A,C and E) and Bl_AlO (B,D and F) acquired on backscattered electron mode. C and D images correspond to the very near surface. E and F images correspond to a region at 50 μm from surface.

-Figure 3. Grazing Incidence X ray Diffraction pattern of polished, BL_ZrO and BL_AlO samples.

- Figure 4. Depth profile of residual stresses in polished, BL_ZrO and BL_AlO samples. Miller index of diffraction planes are indicated.

- Figure 5. Cross section EBSD band contrast image of BL_AlO.

- Figure 6. Microhardnes profile of BL_ZrO and BL_AlO samples.

- Figure 7. Hysteresis loops of BL_ZrO and BL_AlO samples.

- Figure 8. A) Topographic and B) magnetic image obtained by MFM in the cross section of a BL_ZrO sample. The lines mark the edge of the sample.

- Figure 9. MFM images of the cross section of BL_ZrO sample. Images size A) 49.5 µm x 49.5 µm; B) 30.5 µm x 30.5 µm; C) 10.5 µm x 10.5 µm.

- Figure 10. SEM cross-section micrograph obtained at 15 µm from the surface (on the top) of BL_AlO sample and superposed MFM image obtained in the same region from the same sample. Aligned magnetic domains match with the α'-martensite needles. Scale bar is also valid for the superposed image.

Figure 11. A) Topographic and B) magnetic image obtained by MFM in the cross section of BL_AlO sample. The lines mark the edge of the sample. C) MFM images of the two types of magnetic regions observed in this sample: 1- lines with black and white contrast and 2- dark contrast corresponding to single domain crystals (surrounded by solid lines).

4. Table(s)

Table 1. *Characteristics of the particles used for blasting (manufacturer data)*

	BL_ZrO	BL_AlO
Composition	67%ZrO_2, 30% SiO_2, 3% others	99,8 % Al_2O_3
Particle size	125-250 μm	750 μm
Hardness	500-800 HV	2100 HV

5. Figure(s)

Click here to download high resolution image

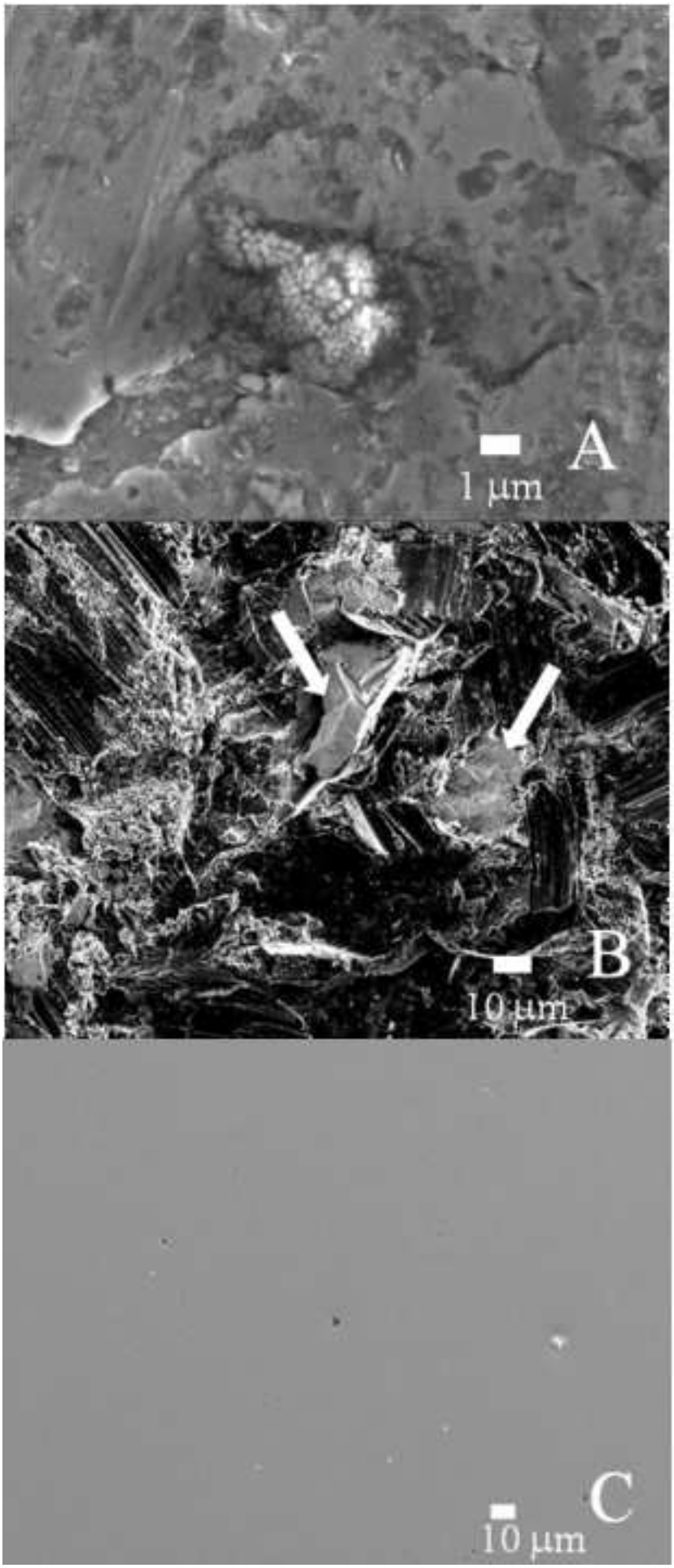

5. Figure(s)

Click here to download high resolution image

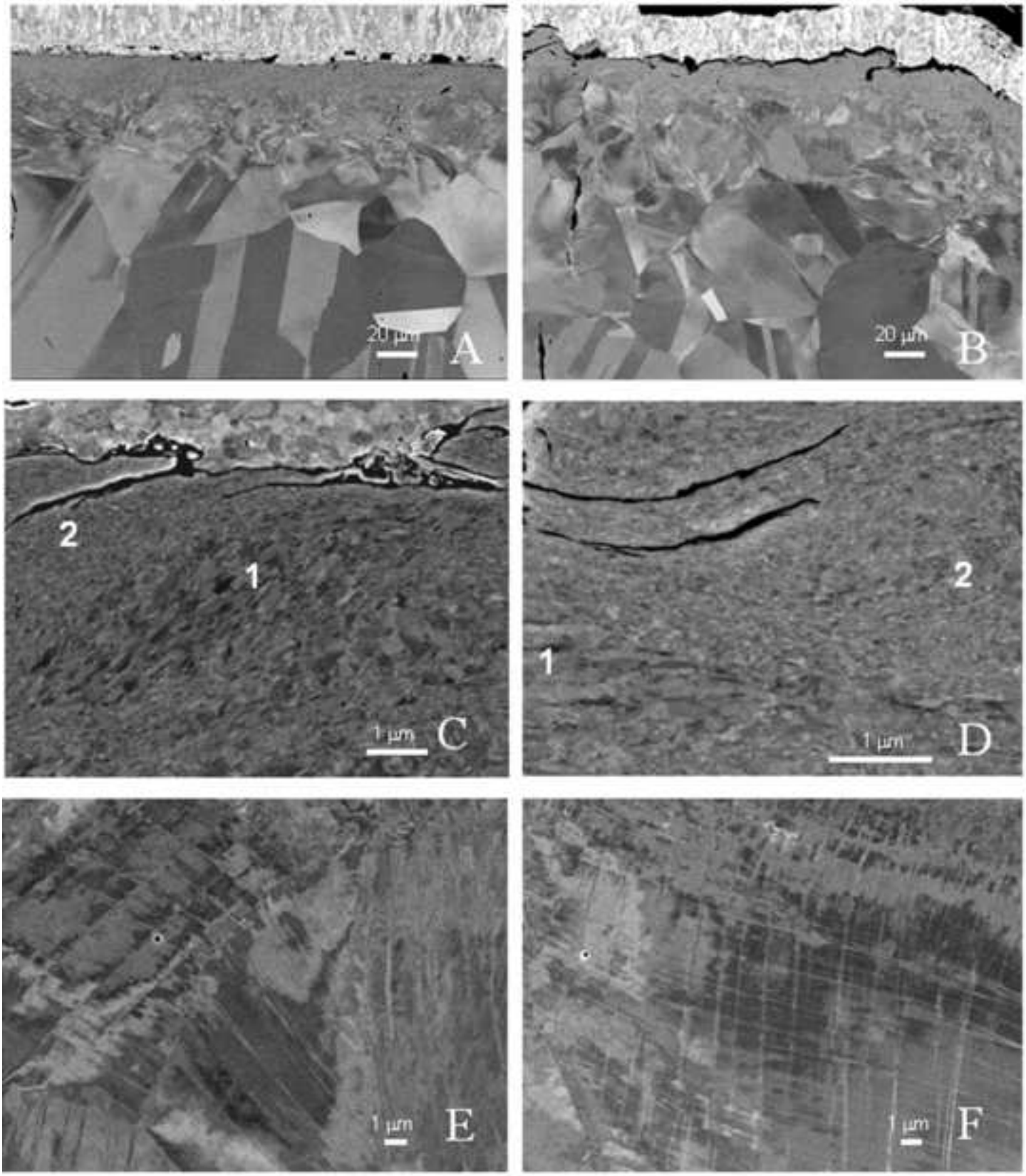

5. Figure(s)

Click here to download high resolution image

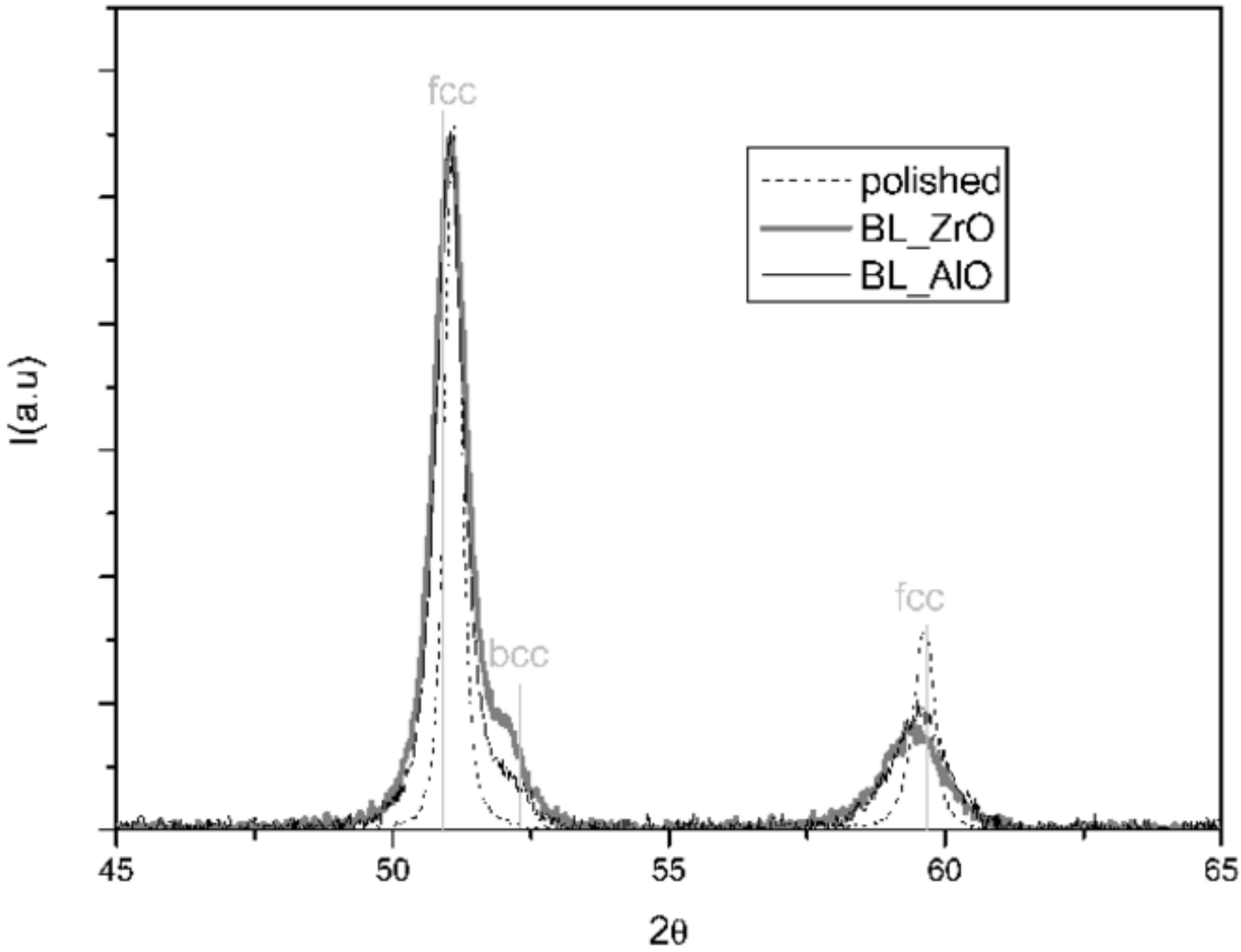

5. Figure(s)

Click here to download high resolution image

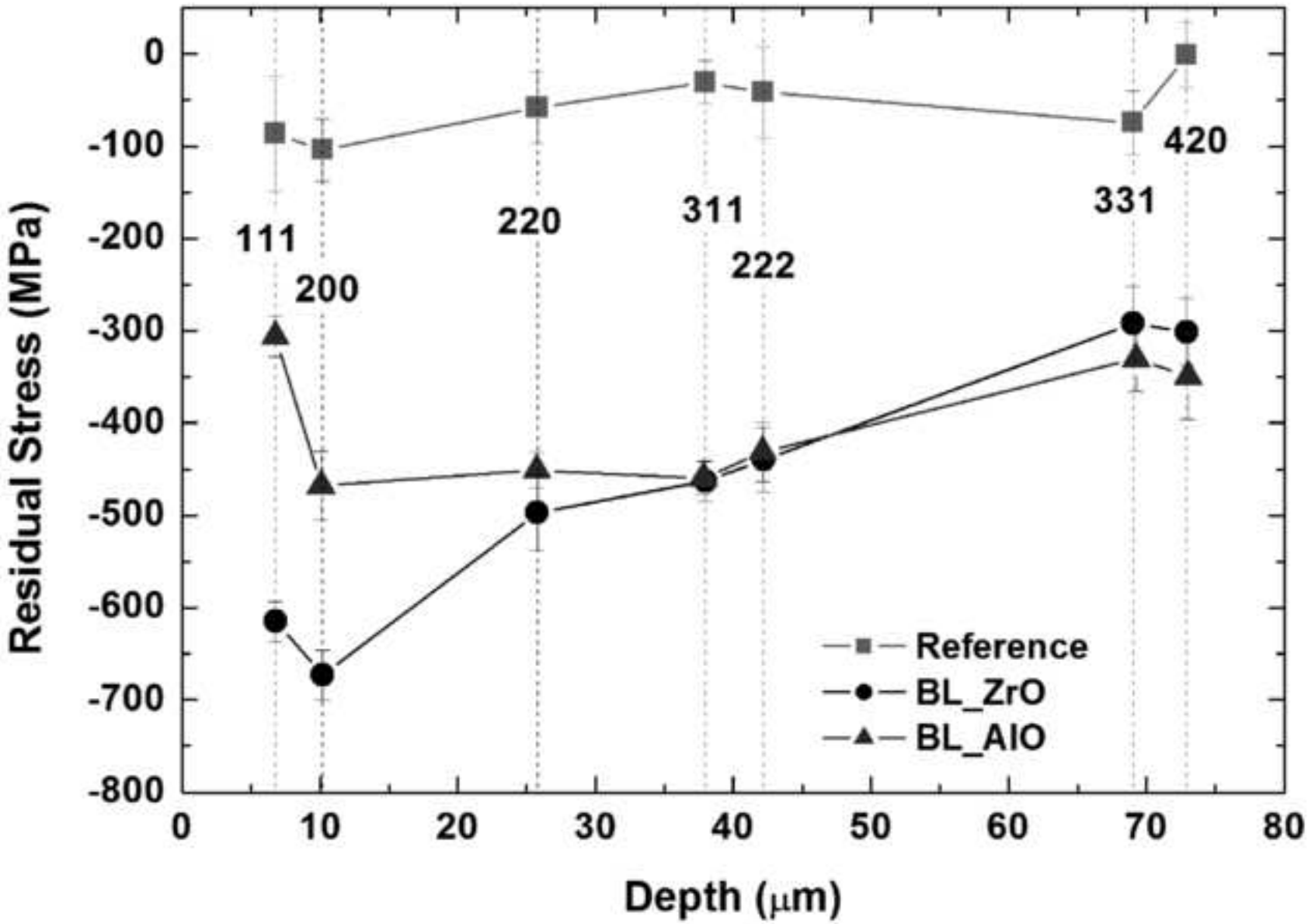

5. Figure(s)

Click here to download high resolution image

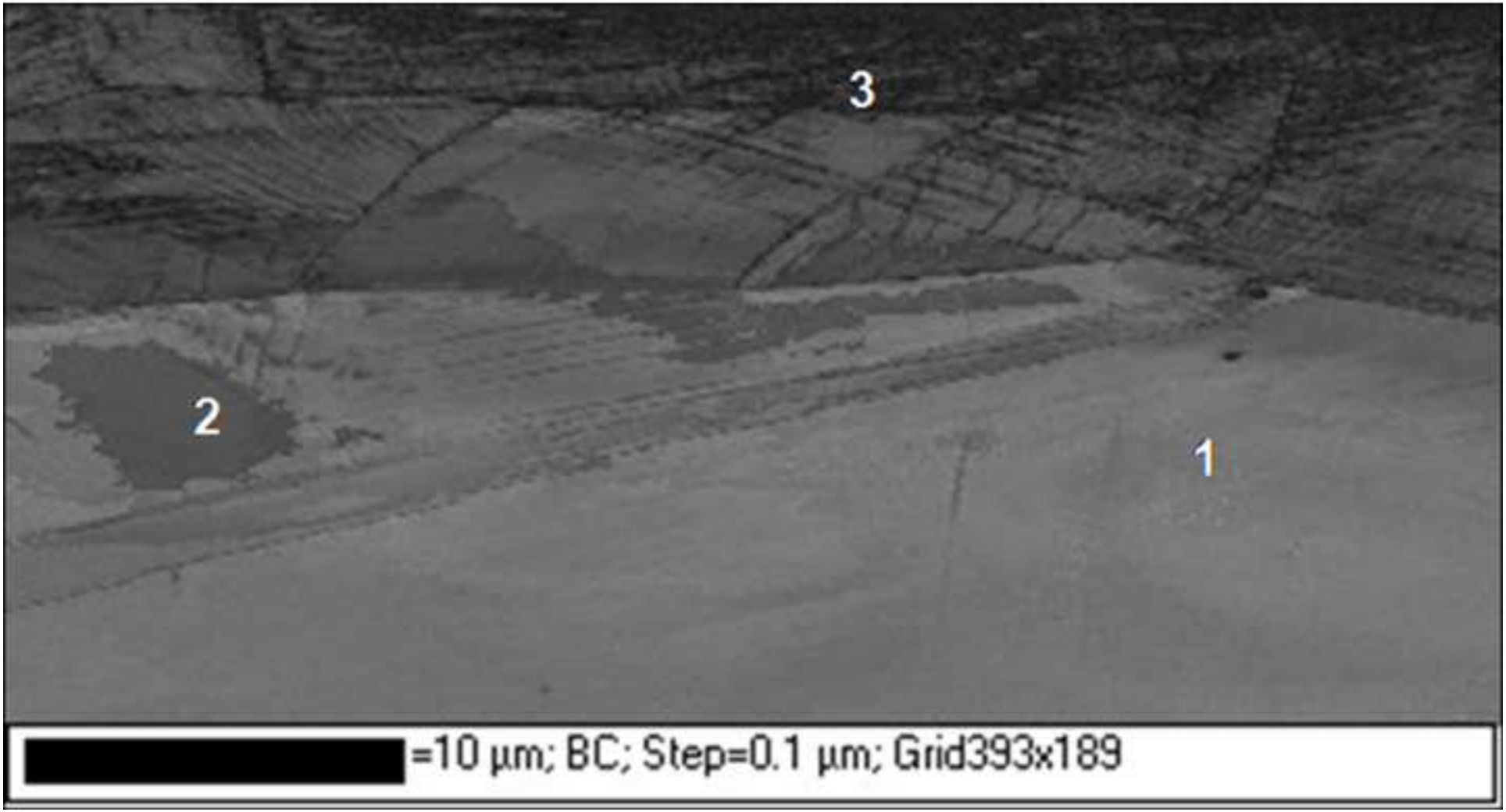

5. Figure(s)

Click here to download high resolution image

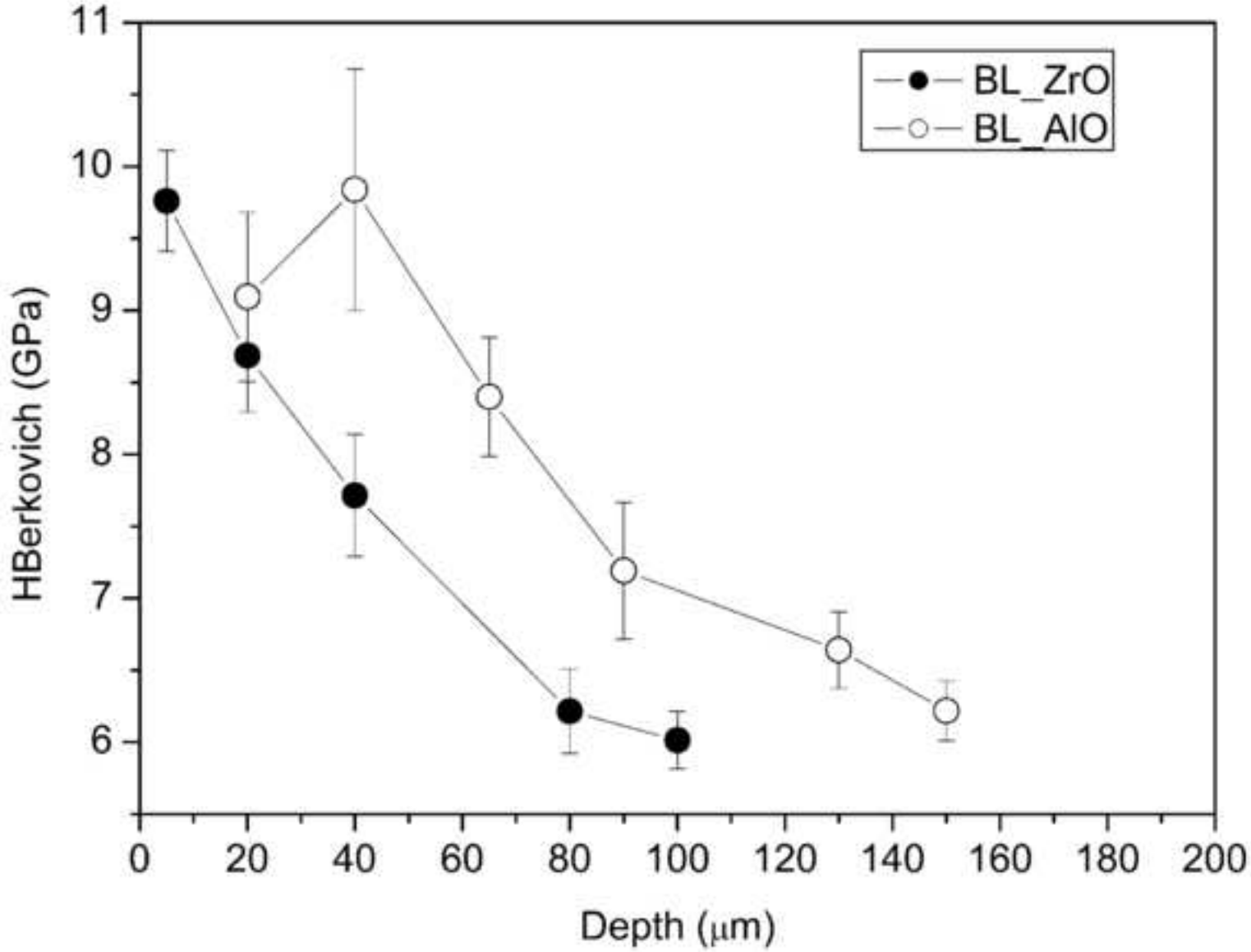

5. Figure(s)

Click here to download high resolution image

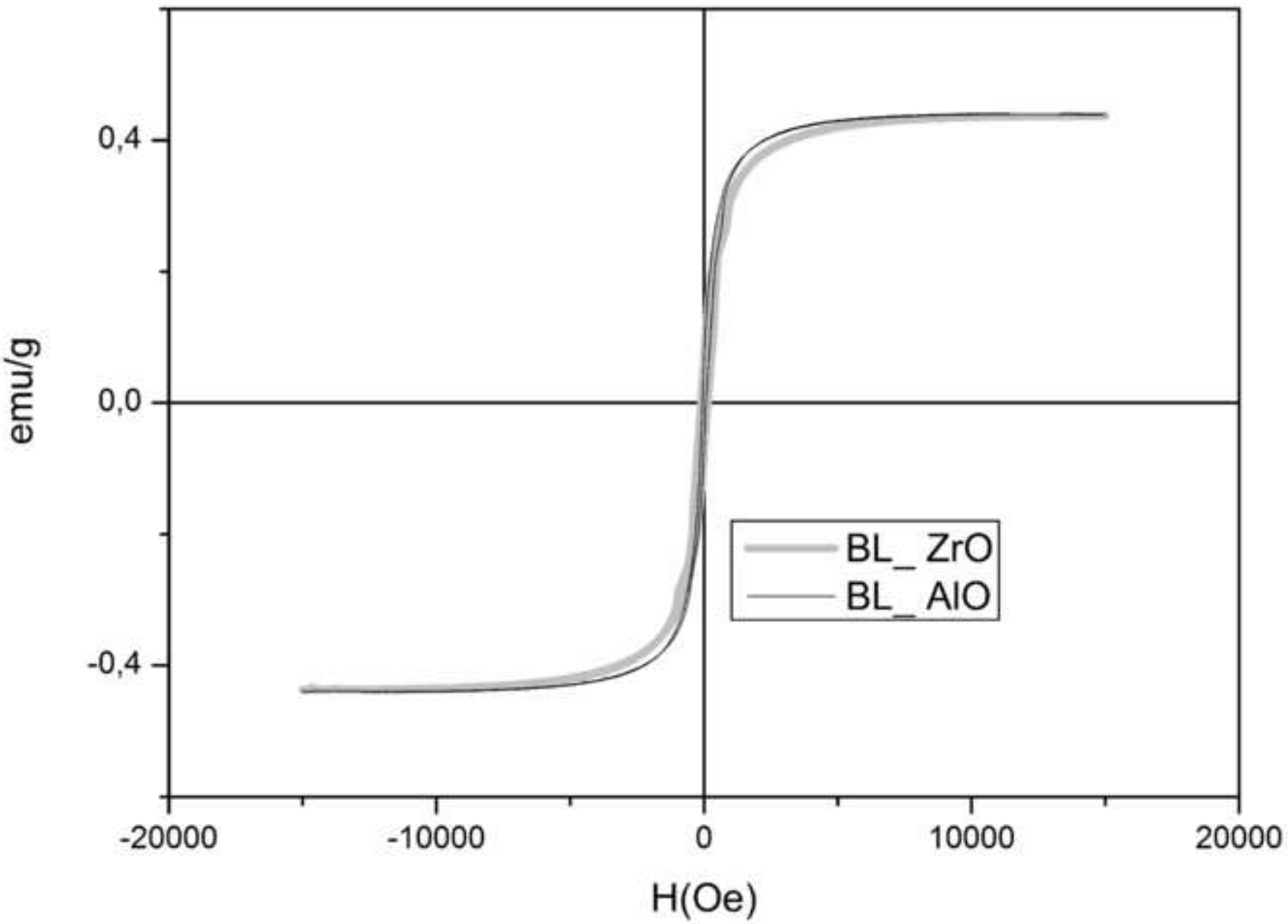

5. Figure(s)

Click here to download high resolution image

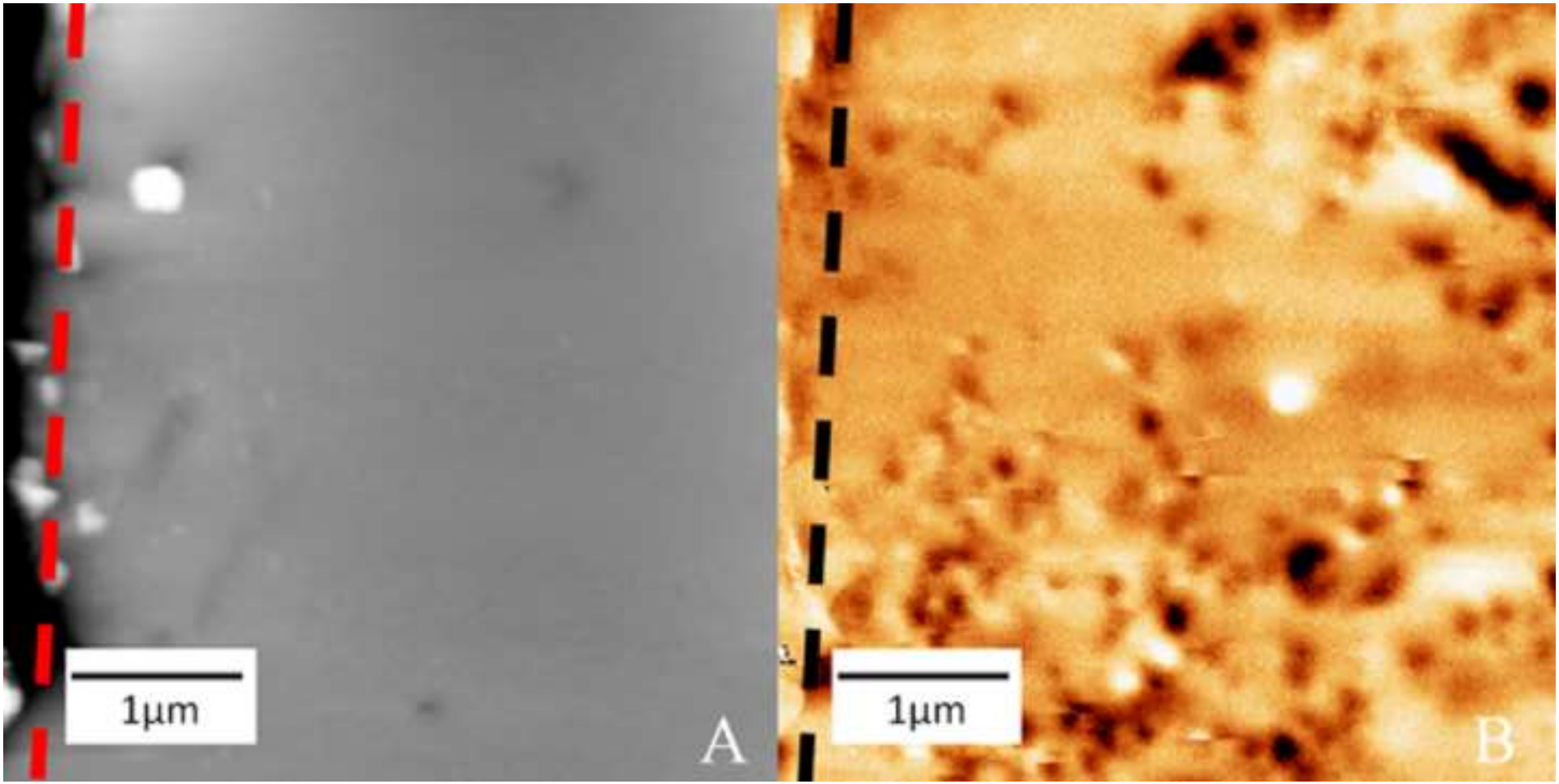

5. Figure(s)

Click here to download high resolution image

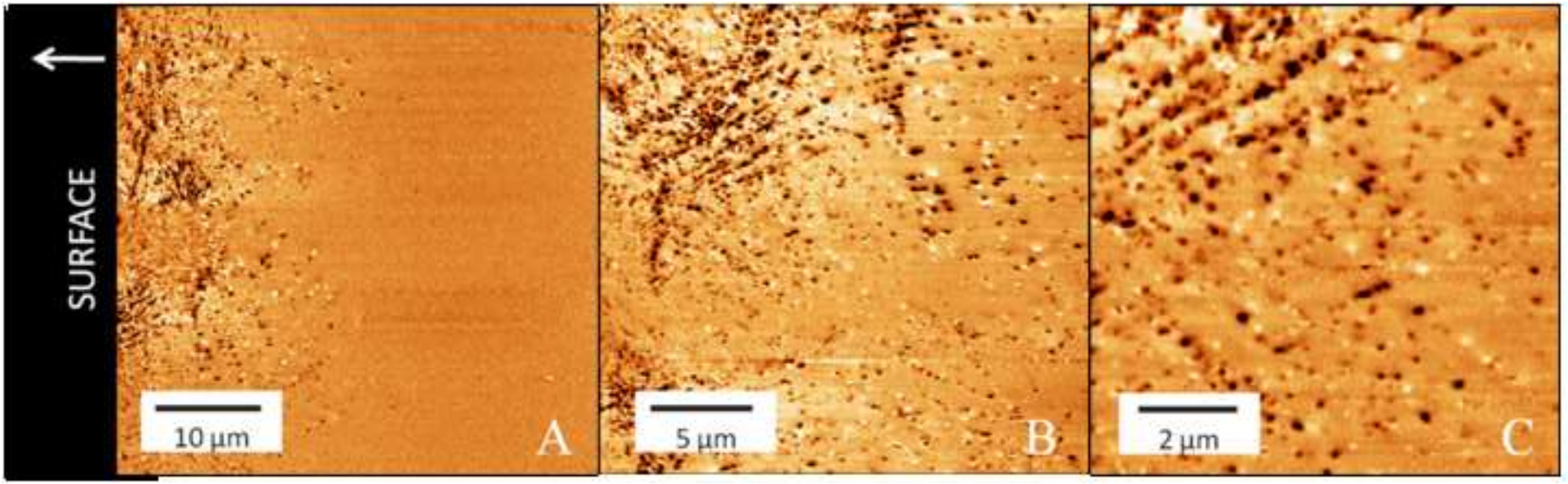

5. Figure(s)

Click here to download high resolution image

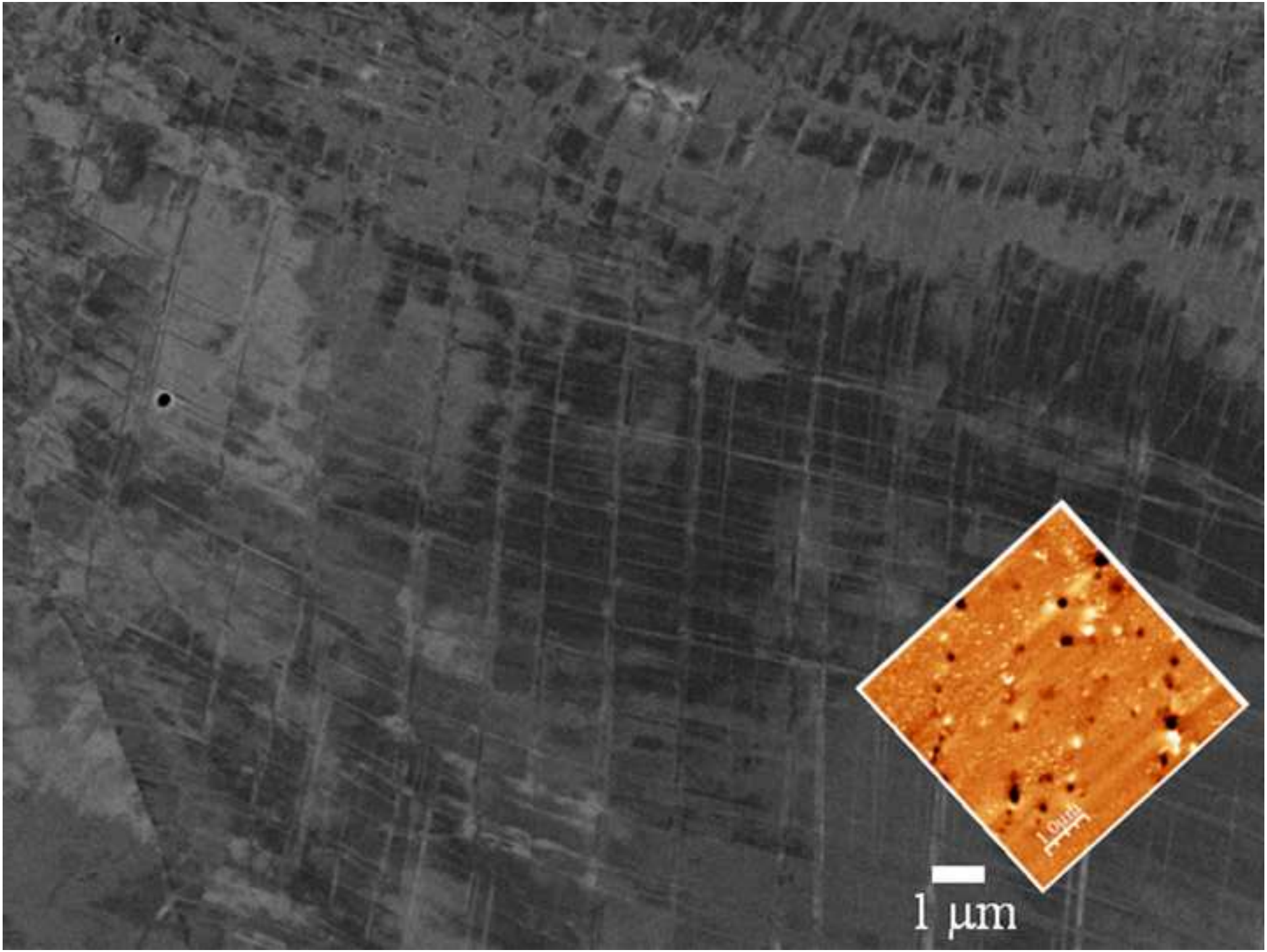

5. Figure(s)

Click here to download high resolution image